Topics in Catalysis (2018) 61:2007–2020
https://doi.org/10.1007/s11244-018-1017-z

ORIGINAL PAPER

The Effect of Si/Al Ratio for Pd/BEA and Pd/SSZ-13 Used as Passive NO_x Adsorbers

Oana Mihai[1,2] · Lidija Trandafilović[1] · Travis Wentworth[1] · Francesc Fluxa Torres[1] · Louise Olsson[1]

Published online: 10 July 2018

Abstract
The mitigation of cold-start emissions involves the development of passive NO_x adsorbers (PNA) systems that store NO_x at low temperature, being designed to release the trapped NO_x at higher temperatures, where downstream NO_x reduction catalysts are efficient. Pd-based zeolites (BEA, SSZ-13) with different SAR (Si-to-Al ratio) were used for PNA investigation, and $Pd/Ce/Al_2O_3$ catalyst was used as a reference for comparison. In this study, NO_x adsorption is investigated at low temperature (80 °C) and it is released during a temperature ramp (to 400 °C) under various gas feed composition. Moreover, detailed characterization was performed using BET, XRD, XPS, TPO, STEM and ICP-SFMS and the stored NO species was studied using in-situ DRIFTS. The addition of CO to the storage mixture resulted in that for Pd/zeolites with low and medium SAR the binding energy for NO was increased. In addition, NO was stored in larger quantities, especially for the Pd/SSZ-13 samples. However, for Pd/BEA (SAR = 300) no such stable NO species was formed and for $Pd/Ce/Al_2O_3$ the CO addition was even negative. Moreover, in-situ NO DRIFTS showed that there was large amount of nitrosyls on ionic palladium for the Pd/zeolites with low and medium SAR, indicating that a significant fraction of the palladium was in ion-exchanged positions, while this peak was small for the Pd/BEA (SAR = 300) and non-existing for $Pd/Ce/Al_2O_3$. Thus, CO addition is beneficial for Pd species that are in ion-exchanged positions, but this is not the case for Pd particles and this can explain the observations that CO is only beneficial for Pd/zeolites with low and medium SAR. Moreover, experiments with similar SAR [Pd/BEA (SAR = 25) and Pd/SSZ-13 (SAR = 24)], showed that there is larger stability of the stored NO_x in the small pore Pd/SSZ-13.

Keywords Palladium · Al_2O_3 · BEA · SSZ-13 · Passive NO_x adsorbers (PNA) · DRIFTS · TPD

1 Introduction

The stringent NO_x emission regulations [1] involve advanced implementation of NO_x reduction techniques, such as NO_x-storage reduction (NSR), also referred as Lean NO_x traps (LNT) [2, 3] and selective catalytic reduction (SCR) [4], in order to control the NO_x emissions from lean-burn engines [5, 6]. However, NSR is not efficient at low temperature since NO oxidation followed by NO_2 storage over alkaline-earth materials or alkali metals must occur. Also, urea SCR has limitations at low temperatures, where one of the major difficulties is that urea cannot be dosed below ca 200 °C, since it otherwise will form deposits such as e.g. biuret [7]. Due to the low temperature limitations of both the NSR and SCR techniques, the NO_x species released during cold-start cannot be converted. An attractive strategy focused on the storage and reduction of NO_x emissions during cold-start is the so-called passive NO_x adsorber [8, 9] (PNA) technology. In this concept, the NO_x is stored at low temperatures and then thermally released once the SCR system reaches its operating temperature. It is important to release the NO_x above 200 °C, however it is also important that the temperature is not too high, because than there is a risk that the PNA is not properly regenerated. Thus, a release temperature between 200 and 300 °C seems to be ideal.

In early studies of passive NO_x adsorbers, Pt/Al_2O_3 [10] as well as Ag/Al_2O_3 [9, 11] were studied. However, the Pt/

✉ Louise Olsson
louise.olsson@chalmers.se

[1] Chemical Engineering; Competence Centre for Catalysis, Chalmers University of Technology, 412 96 Gothenburg, Sweden

[2] Department of Petroleum Processing Engineering and Environmental Protection, Petroleum-Gas University of Ploiesti, 39 Bucuresti Blvd., 100680 Ploiesti, Romania

Al_2O_3 sample releases most of the NO_x below 200 °C or above 350 °C, which is not in the optimum interval. Moreover, the silver based catalysts required that small amounts of hydrogen was present, which is a limitation [9]. In a patent by Johnson Matthey [12], Pd and CeO_2 containing catalysts showed interesting properties, where NO_x was stored below temperature of 200 °C and released above this temperature. However, Pd/CeO_2 exhibit low NO_x storage and in addition has large problems with sulfur adsorption [13].

Chen et al. [13] found that Pd/zeolites were very promising materials for PNA applications. Moreover, Theis and Lambert [14] found that the presence of C_2H_4 improved the NO_x storage after thermal aging of the PNA. The zeolite structure plays a key role in the NO adsorption ability on the Pd sites, and Pd on MFI, CHA, and BEA zeolites showed considerable NO_x storage and desorption efficiencies [13]. However, Pd/BEA was better than the other investigated zeolites in terms of NO_x storage at 100 °C or lower and NO_x release above 200 °C [13]. Using several characterization techniques Zheng et al. [15] examined Pd/BEA, Pd/ZSM-5 and Pd/SSZ-13 and found that there are multiple Pd species on the Pd/Zeolites; Pd in the cationic sites of zeolites and PdO_2 and PdO particles on the external surface. They also concluded that in the small pore zeolites there are more particles on the outside due to sterical hindrance [15]. However, high temperature treatment (750 °C) resulted in an increased amount of atomically dispersed Pd in Pd/ZSM-5 [16]. Moreover, Lee et al. [16] found that the Si/Al loading in ZSM-5 was important for the NO storage and an optimum of Si/Al ratio of 30 was found. Vu et al. [17] found that the addition of CO to the feed during NO storage results in an increase in the temperature for NO_x release over Pd/BEA. The effect of CO is to reduce the palladium and metallic Pd, "naked" Pd^{2+}, and Pd^{+} sites are the active sites for NO adsorption in the presence of CO [15]. Different Pd based zeolites have been examined, and it is clear that different zeolites results in different NO storage and release behavior, where Pd/BEA is the best at low adsorption temperature and Pd/SSZ-13 at higher temperatures [15]. Moreover, for Pd/ZSM-5 it is also found that the Si/Al ratio is critical in PNA experiments without CO presence [16]. However, there are to our knowledge, no studies available where the effect of Si/Al ratio on Pd/BEA and Pd/SSZ-13 is studied. Moreover, there are no studies presented where the effect of Si/Al ratio on Pd/zeolites are examined in the presence of CO, which is significantly changing the adsorption and desorption characteristics [15].

The objective of the present work is therefore to study the effect of different Si/Al ratio on the Pd/BEA and Pd/SSZ-13, with and without the presence of CO. This is done through NO temperature desorption (TPD) experiments in various gas mixtures. The catalysts are thoroughly characterized using BET, ICP-SFMS, XRD, TPO, STEM, XPS and in-situ DRIFT spectroscopy to study the adsorbed NO species. In addition, a $Pd/Ce/Al_2O_3$ catalyst was examined as a reference sample.

2 Experimental

2.1 Catalyst Synthesis

2.1.1 $Pd/Ce/Al_2O_3$ as a Reference Sample

A 1%Pd/8%Ce/Al_2O_3 catalyst was prepared as a reference material. The γ-Al_2O_3 (Puralox SBa-200, Sasol, pre-calcined at 750 °C, for 2.5 h, 4 °C/min), an aqueous solution of $Pd(NO_3)_2$ (Heraeus GmbH, 16.37 wt% Pd) and Cerium(III) nitrate hexahydrate (Sigma Aldrich) were used as starting materials. The desired amount of Cerium(III) nitrate hexahydrate, corresponding to 8 wt% Ce was loaded in two steps (each of 4 wt% Ce) by incipient wetness impregnation method, with drying between each step. The Ce nitrate was dissolved in purified deionized "MilliQ" water (Millipore) and the aqueous solution was dropwise added to the alumina support. After the sample was dried at 100 °C overnight and calcined at 500 °C for 5 h, a corresponding amount of Pd precursor (to reach 1 wt%) was dissolved in an appropriate amount of "MilliQ" water and was impregnated on the Ce/Al_2O_3. After the addition of the Pd solution, the resulting powder was dried and calcined at same conditions as described above.

2.1.2 Pd/SSZ-13

The hydrothermal synthesis of Na-SSZ-13 was performed based on the method described by McEwen et al. [18]. Starting materials used for the synthesis was sodium silicate solution (Sigma-Aldrich), TMAAI 25% solution of tricyclo [3.3.1.13, 7] decan-1-aminium,*N,N,N*-trimethyl-hydroxide (Sachem, ZeoGen SDA), zeolite Y CBV712 (Zeolyst International) and NaOH (Sigma-Aldrich). The obtained Na-zeolite sample was calcined at 550 °C for 8 h with a ramp of 0.5 °C/min. In the next step, Na-SSZ-13 was ion-exchanged with NH_4NO_3, following a detailed procedure described by Olsson et al. [19]. The H-form of SSZ-13 was obtained by calcination of NH_4-form in air for 4 h at 550 °C with a ramp rate of 5 °C min^{-1}. The Pd/SSZ-13 was synthesized using incipient wetness impregnation with the appropriate amounts of Pd precursors corresponding to 1 wt% Pd. After the Pd solution had been added, the resulting powder was dried at 100 °C overnight and calcined at 500 °C for 5 h with 2 °C/min.

Moreover, in order to prepare a SSZ-13 with higher SAR (SiO_2/Al_2O_3) ratio was instead zeolite Y CBV780 (Zeolyst International) used as starting material. NH_4- and H- and

Pd- forms of SSZ-13 were prepared using the same procedure as described in previous paragraph.

2.1.3 Pd/BEA

Beta zeolite (CP814E, SAR 25; CP814C, SAR 38, and CP 811-300, SAR 300, Zeolyst International) were used as support for impregnation of Pd precursor. Same procedure as mentioned in Sect. 2.1.2 was followed for the synthesis. For simplification, the catalysts used in this work are summarized in Table 1.

2.2 Monolith Preparation

The monoliths were cut from a commercial honeycomb cordierite structure (20 mm in length, 21 mm in diameter, 400 cpsi) and then heated to 500 °C for 2 h. The monolith substrates were coated using slurry consisting of 20 wt% solid phase and a liquid phase of ethanol and water (1:1). The catalyst and Disperal P2 (boehmite binder) ratio in the solid phase was 95:5 based on weight. Each time after dipping the monolith, the excess slurry was removed and the monolith dried in air for 2 min at 90 °C. The procedure was repeated several times until the desired amount of washcoat (~ 750 mg) was reached after which the monoliths were calcined in air at 500 °C for 5 h, 2 °C/min ramp.

2.3 Catalyst Characterization

The BET surface area and pore volume were determined by measuring N_2 adsorption isotherms at the temperature of liquid N_2 (− 195 °C) using a Tristar 3000 (Micromeritics) instrument. Prior to the measurement, the samples were degassed at 220 °C for 3 h under vacuum.

Elemental analysis was used for determining the Si/Al ratio of the SSZ-13 samples. This was done by inductively coupled plasma sector field mass spectrometer (ICP-SFMS) and the measurements were performed by ALS Scandinavia AB.

Table 1 Summary of prepared catalysts

Catalyst type	Support	SAR (SiO_2/Al_2O_3 ratio)	Metal loadings (wt%)	
			Pd	Ce
$Pd/Ce/Al_2O_3$	γ-Al_2O_3	–	1	8
Pd/SSZ-13	SSZ-13	12		–
		24		
Pd/BEA	BEA	25		
		38		
		300		

XRD was performed using a powder diffractometer (BrukerAXS D8 advance) with Cu Kα source (λ = 1.542 Å) operating at 40 kV and 40 mA.

X-ray photoelectron spectroscopy (XPS) measurements were done on a Perkin Elmer PHI 5000C ESCA system equipped with a monochromatic Al K X-ray source with a binding energy of 1486.6 eV. All binding energies were referenced to a C 2s BE of 284.8 eV. Note that the samples experienced variable degrees of charging and a neutralizer with emission control (21.8) was therefore used to minimize this charging. PdO from Sigma Aldrich (99.97% trace metals basis) were used as reference material.

A transmission electron microscopy (TEM) analysis was performed to examine the Pd particle size for fresh samples and samples scraped from monoliths after flow reactor experiments. The powder of the sample was placed on carbon films using TEM Cu grids. The particles were imaged using an FEI Titan 80-300 microscope equipped with a field emission gun (FEG), a probe Cs (spherical aberration) corrector and a Gatan image filter (GIF) (Tridium) operated at an acceleration voltage of 300 kV. The images were recorded using a high angle annular dark field (HAADF) detector in the scanning TEM imaging mode (STEM).

2.4 Flow Reactor Experiments

2.4.1 Temperature-Programmed Desorption (TPD) Experiments

The TPD experiments were performed in a flow reactor setup. It consisted of a horizontal quartz tube (70 cm length, 22 cm inner diameter), gas dosing system using several mass flow controllers (MFC, Bronkhorst), an evaporation mixing system for controlling water vapor flow (CEM, Bronkhorst) into which the monolith was inserted. Two type-K thermocouples were used to measure the temperature in the gas flow before the catalyst and in the center of the middle channel. A gas Fourier transform infrared (FTIR) spectrometer (MKS Multigas 2030) was connected to the outlet of the reactor for monitoring the concentrations of the gases. The lines prior to and after the reactor were heated to 200 °C and insulated in order to prevent water condensation during measurements. Argon was used as inert balance gas. The total flow was 750 ml min^{-1} during the TPD experiments, whereas a flow of 3300 ml min^{-1} was employed for pretreatment of the samples.

In this study, several TPD procedures were applied (marked as TPD 1, TPD 2, etc.), as listed in Table 2. In order to obtain stable activity, the catalysts were first degreened using 500 ppm NO, 5% CO_2, 8% O_2 and 5% H_2O at 500 °C for 1 h with the total flow of 3500 ml min^{-1}. Prior to each TPD experiment the catalyst was pre-treated at 400 °C, using the following three sequences: (1) 1% H_2, 5% CO_2 and 5%

Table 2 Experimental procedure for TPD experiments

TPD[a]	Adsorption		Desorption	
	Gas composition	Temperature (°C)/time (min)	Isothermal, 80 °C, for 15 min	Ramp to 400 °C, 20 °C/min
1	$NO+O_2$	80/30	O_2+Ar	
2	$NO+O_2+H_2O$		O_2+H_2O+Ar	
3	$NO+O_2+H_2O+CO_2$		$O_2+H_2O+CO_2+Ar$	
4	$NO+O_2+H_2O+CO_2+CO$		$O_2+H_2O+CO_2+Ar$	

[a]The NO, O_2, CO_2, CO and H_2O were present in the concentrations of 200 ppm, 8%, 5%, 400 ppm and 5%, respectively in all TPD tests

H_2O for 15 min; (2) 5% CO_2 and 5% H_2O for 5 min; (3) 5% CO_2, 8% O_2 and 5% H_2O for 20 min. After pretreatment, the samples were cooled to the target temperature (80 °C) under (O_2+Ar) for TPD1, (O_2+H_2O+Ar) for TPD2, ($O_2+CO_2+H_2O+Ar$) for TPD3 and TPD4. The TPD procedure consisted of an adsorption of 200 ppm NO in the presence of O_2, H_2O, CO_2 and CO (see Table 2 for details) with an Argon balance at 80 °C for 30 min. Thereafter, at the same temperature as the adsorption step, the catalyst was flushed with a specific gas mixture for each TPD (see Table 2) for 15 min to remove loosely bound species from the surface. The temperature was then linearly increased to 400 °C at a ramp speed of 20 °C min^{-1} and finally, the temperature was kept at 400 °C for 10 min.

2.4.2 Temperature-Programmed Oxidation (TPO) Experiments

TPO experiments were conducted in a Setaram Sensys DSC (Digital Scanning Calorimeter) using Ar as the inert balance. About 60 mg of the powder sample was loaded in the quartz tube reactor (inner diameter of 5 mm), which was mounted in an electrical furnace as part of calorimeter. In order to pretreat the catalytic surface, the samples were first reduced for 30 min at 500 °C in 1% H_2 and subsequently cooled down to 100 °C in the same reducing atmosphere. After the catalysts were flushed with Ar for 25 min at 100 °C, the TPO tests were started when 500 ppm O_2 was introduced into the system and the catalysts were flushed with 500 ppm O_2 for 90 min. Thereafter, oxidation was carried out by heating the samples from 100 to 800 °C (with a ramp rate of 20 °C/min), while exposing the samples to 500 ppm O_2 in Ar. When the temperature reached 800 °C, the catalysts were kept for 60 min in O_2 atmosphere and then the system was cooled down to room temperature in the same environment.

2.5 In-situ DRIFT Spectroscopy

The surface species on the samples were characterized during NO adsorption conditions by in-situ DRIFT spectroscopy. The measurements were performed using a Bruker Vertex 70 FTIR spectrometer equipped with a high-temperature reaction cell (Harrick Scientific). Approximately 70 mg of catalyst powder was placed on a porous grid in the sample cup. The sample was covered by a dome equipped with two KBr windows, and reactant gases were flown through the sample using Bronkhorst mass flow controllers. After placing the samples in the reaction cell, each sample was degreened at 550 °C for 1 h in 8% O_2, 1000 ppm NO and 1% H_2O. After degreening, the samples were pretreated at same temperature in 8% O_2 and 1% H_2O for 30 min and then cooled down to 80 °C in same atmosphere. At this temperature, a background was first acquired under 8% O_2 and 1% H_2O, Ar balanced. After taking background, 1000 ppm NO was introduced in the flow in the presence of 8% O_2 and 1% H_2O for 30 min. A resolution of 4 cm^{-1} was adapted and the data are presented as absorbance (logI/R).

3 Results and Discussion

3.1 Catalyst Characterization

The SiO_2/Al_2O_3 ratios, denoted SAR, for the synthesized SSZ-13 materials were determined using ICP-SFMS, which resulted in SAR of 12 and 24, respectively. Moreover, the Na content was below detection limit in the samples. In addition, BET surface areas were measured and resulted in 167.3, 624.6, 669,7, 582.9 and 579.5 for Pd/Ce/Al_2O_3, Pd/SSZ-13 (SAR = 12 and 24) and Pd/BEA (SAR 38 and 300), respectively. According to N_2 physisorption data, it can be seen that the BET surface area of the Pd/Ce/Al_2O_3 catalyst was lower [20], which is expected since alumina support has lower surface area compared to zeolites in general. Highest BET specific surface areas are revealed for small-pore-sized SSZ-13-based materials [21].

Figure 1 shows the diffraction patterns of the calcined zeolite catalysts. Analysis of XRD patterns recorded for the zeolite materials presented in Fig. 1 clearly show the structures of the SSZ-13 [22] (Fig. 1a) and BEA [23, 24] (Fig. 1b). In the case of Pd/SSZ-13 (Fig. 1a), it showed the characteristic of CHA topology with the diffraction peaks matching well with the standard diffraction of zeolite SSZ-13 from (1 0 0), (1 0 − 1), (− 1 1 − 1), (1 1 1), (1 0 − 2), (0

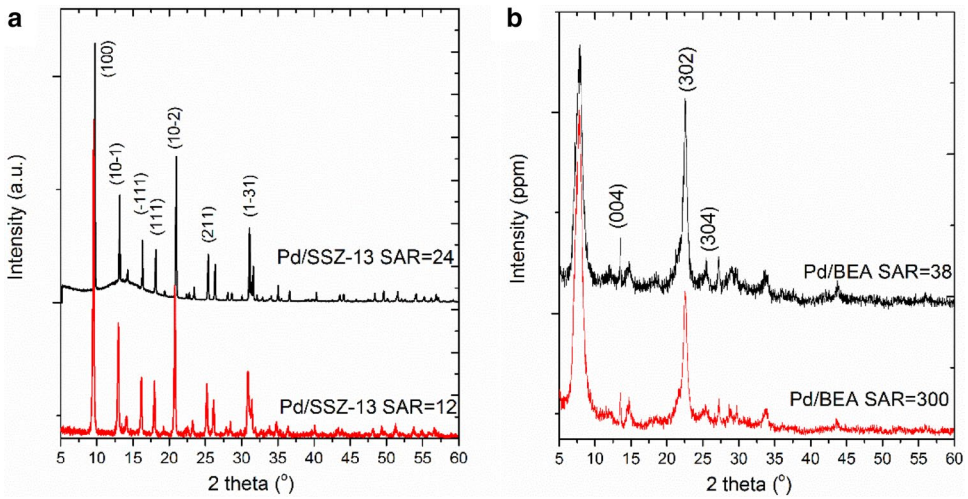

Fig. 1 XRD patterns of **a** Pd/SSZ-13 with SAR (SiO_2/Al_2O_3) of 12 and 24; **b** Pd/BEA with SAR of 38 and 300

−2 2), (1 −3 1) and (3 1 0) crystal [25, 26]. While the Pd/BEA (SAR 38 and 300) diffraction peaks are identified as (004), (302) and (304) [27]. As it can be seen from Fig. 1 changing of SAR in zeolite structure did not cause any significant changes of the position of the peaks.

The morphology of the calcined Pd/BEA (SAR = 300) and Pd/SSZ-13 (SAR = 24) was investigated by TEM and the HAADF-STEM micrographs at various magnifications are shown in Fig. 2. Palladium particles can be seen as bright spots and it is clear that the Pd/BEA (SAR = 300) shows many and quite large Pd particles (Fig. 2a). This is expected since the SAR ratio is very high; there is only few ion-exchange positions available, which results in Pd particles. Figure 2b presents STEM images of Pd/SSZ-13 (SAR = 24). Also, for Pd/SSZ-13 it is clear that there are Pd particles available on the surface, however they are significantly smaller. The size of Pd particles for Pd/BEA (SAR = 300) are in the range from 24 till 51 nm, while for Pd/SZZ-13 (SAR = 24) particle size have range from 1.7 till 5 nm with the majority of particles size around 2–3 nm. The size differences between Pd/BEA (SAR = 300) and Pd/SSZ-13 (SAR = 24) are probably due to the different SAR. Smaller SAR of Pd/SSZ-13 is giving more ion-exchanged positions which results in more well dispersed Pd species (Fig. 2).

The effect of running of flow reactor experiments on the Pd particles size's for Pd/BEA (SAR = 300) is examined. In Fig. 3, the results from scrapped of catalysts from used monolith are shown, with M denoting sample taken from

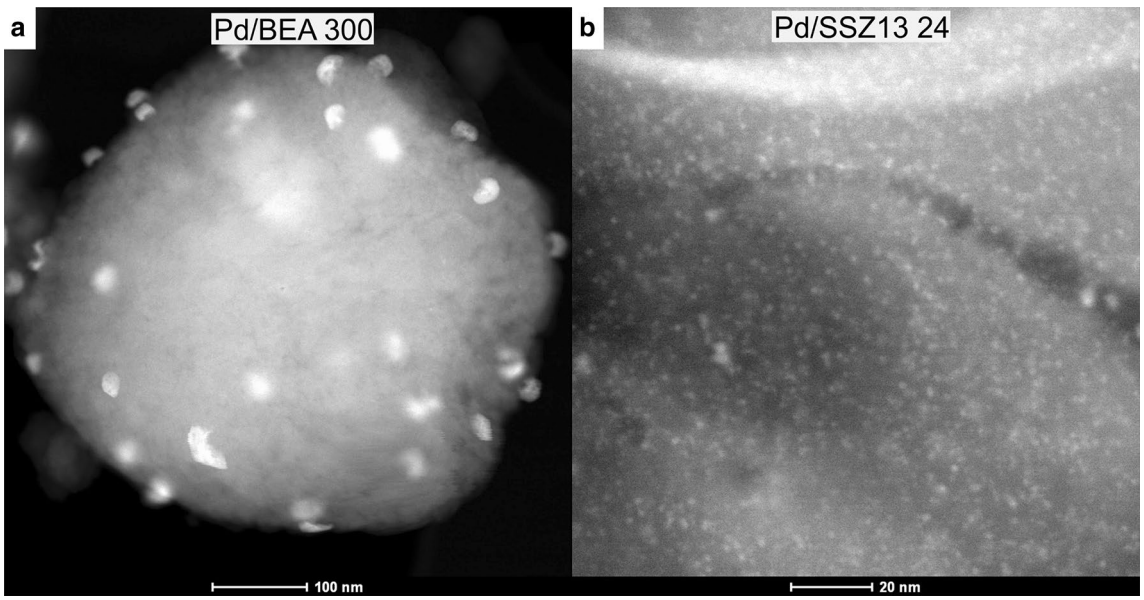

Fig. 2 **a** STEM images of the Pd/BEA (SAR = 300) at 100 nm; **b** STEM images of Pd/ SSZ-13 (SAR = 24) at 20 nm

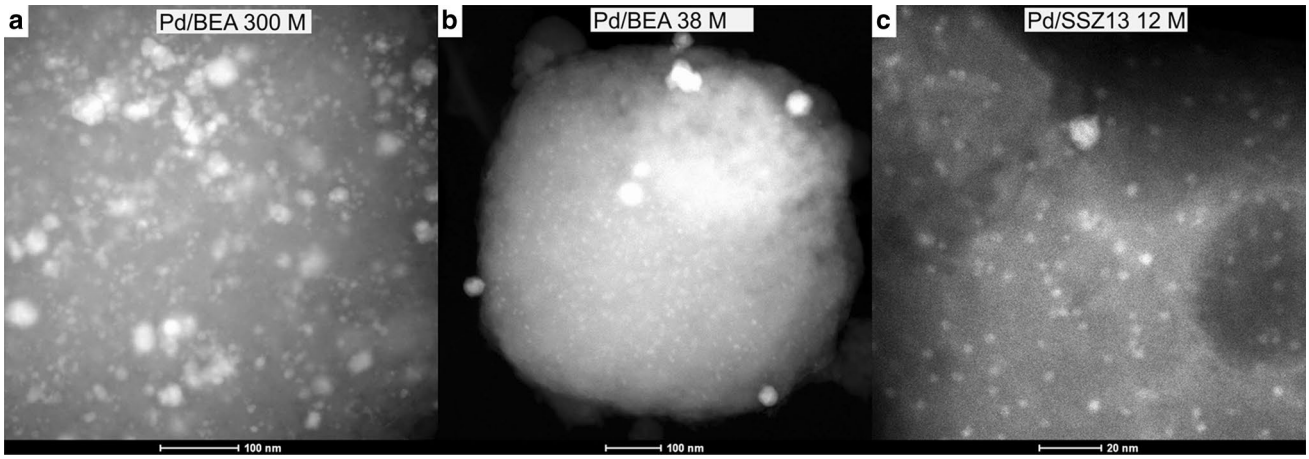

Fig. 3 **a** STEM images of the Pd/BEA (SAR = 300) at 100 nm; **b** Pd/BEA (SAR = 38) at 100 nm and **c** Pd/ SSZ-13 (SAR = 12) at 20 nm. Scrapped off powder from used monoliths are used

monoliths. As it can be seen from Fig. 3a Pd particles for Pd/BEA (SAR = 300) M are now more dispersed with size ranging from 8 till 40 nm. These results were found on several images on different positions. These results indicate that during flow reactor experiments of Pd/BEA (SAR = 300) the Pd dispersion improved, and this is similar as found for solid state ion-exchange of Cu/SAPO-34 [28]. In the case of Pd/BEA (SAR = 38) M the size of a particles are from the 11 till 14 nm with quite even distribution. Comparing the particle sizes for Pd/BEA (SAR = 38) M and Pd/BEA (SAR = 300) M we can see that lower SAR gives the smaller particles. For Pd/SSZ-13 (SAR = 12) M the particles size is in the range from 2 till 5 nm (see Fig. 3c), which is similar to the size range fresh Pd/SSZ-13 (SAR = 24, presented in Fig. 2b) leading to conclusion that particles are not drastically influenced by SAR and experimental treatment in the case of Pd/SSZ-13 samples.

The oxidative properties of the prepared samples were investigated through TPO tests and the obtained results are shown in Fig. 4. In case of $Pd/Ce/Al_2O_3$, the oxidation started at about 120 °C, with the maximum oxygen consumption peak at 301 °C. This behavior is related with the Pd oxidation to PdO and ceria oxidation, and is similar to the max adsorption temperature (359 °C) that was obtained on $Pt/Pd/Ce/Al_2O_3$ by Sadokhina et al. [29]. Moreover, at high temperature an oxygen release is visible with a peak maximum at 768 °C, which is due to palladium oxide decomposition.

For all Pd/zeolites the oxidation occurs at higher temperature compared to the $Pd/Ce/Al_2O_3$ sample. The Pd/BEA (SAR = 38) and Pd/BEA (SAR = 25) have similar oxygen uptake profiles, with maximum around 401 °C (see Fig. 4a). Interestingly, the Pd/BEA with the higher SAR (SAR = 38) released oxygen, indicating decomposition of palladium oxides, while Pd/BEA (SAR = 25) did not. In Fig. 4b, the Pd/

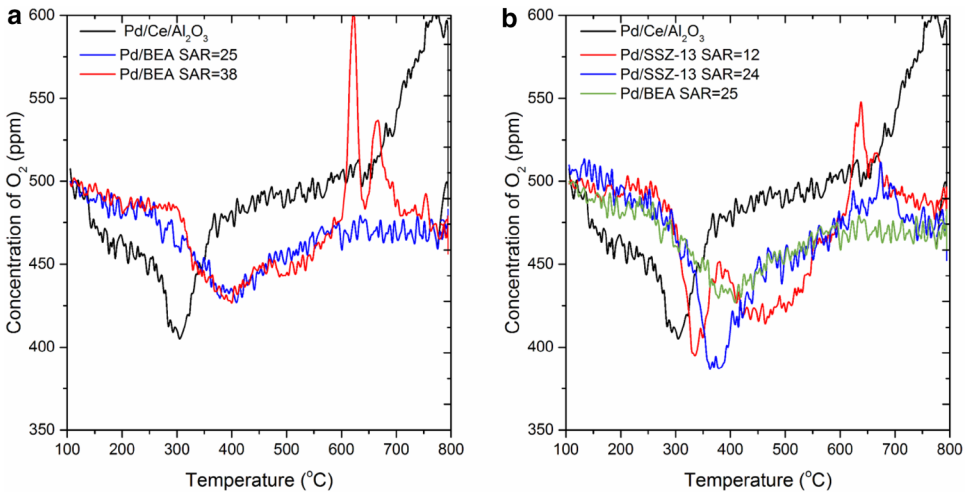

Fig. 4 TPO tests over **a** Pd/BEA (SAR = 25 and 38) and **b** Pd/SSZ-13 (SAR = 12 and 24), while $Pd/Ce/Al_2O_3$ is base case reference catalyst. Prior to the TPO experiment, the samples were reduced for 30 min under 1% H_2 in Ar at 500 °C

BEA (SAR = 25) is compared with Pd/SSZ-13 (SAR = 24), and it is clear that Pd/SSZ-13 has larger oxygen uptake. For the lowest SAR, Pd/SSZ-13 (SAR = 12) two clear adsorption peaks are observed at 338 and ca 475 °C, which indicate that different palladium species are available that are being oxidized. Moreover, the O_2 release temperature for Pd/BEA (SAR = 38) and Pd/SSZ-13 (SAR = 12) are both lower compared to Pd/Ce/Al_2O_3, indicating that some of the oxygen on these catalyst are loosely bound. However, the desorbed amount is much lower for the Pd/zeolites than Pd/Ce/Al_2O_3, showing that the majority of the oxygen binds strongly.

XPS analysis was performed in order to examine the Pd oxidation states in the Pd/zeolite samples. The existence of Pd(II) over Pd/SSZ-13 and Pd/BEA catalysts (Fig. 5a, b) is revealed by XPS measurement of PdO sample used as reference and is presented in the lower panels in Fig. 5a, b. The peak positions for Pd(II) from PdO sample located at 337 eV ($3d_{5/2}$) and 342.4 eV ($3d_{3/2}$) were taken as the basis for deconvolution of XPS spectra. The values for Pd(IV) taken from the work of Zeng et al. [15] at 338.9 eV ($3d_{5/2}$) and 344.3 eV ($3d_{3/2}$), together with Pd(II) were used for deconvolution of experimental spectra presented in Fig. 5 with dashed red line. The calculated percentages of Pd(II) and Pd(IV) from spectra deconvolution reveal that Pd(II) dominate in all samples, which is also seen by comparing the spectras from the catalysts with the reference material. Both Pd/BEA samples, as well as Pd/SSZ-13 (SAR = 12) show similar amount of Pd(IV), between 25 and 32%. The Pd/SSZ-13(SAR = 24), shows higher amount of Pd(VI) (49%), but it should be noted that there are some uncertainties in the deconvolution due to low Pd signal in XPS, because of low Pd amount.

3.2 NO Adsorption Using In-situ DRIFT Spectroscopy

In order to further characterize the Pd species NO DRIFTS experiments were conducted. The DRIFTS spectra when adding NO to O_2 and H_2O gas mixture over Pd/Ce/Al_2O_3 are presented in Fig. 6. The large bands between 1200 and 1600 cm^{-1} can be associated with different NO based species, such as: bridged nitrates at 1614 and 1232 cm^{-1} (1606 and 1249 cm^{-1} [30]), bidentate nitrates at 1545 cm^{-1} (1530–1540 cm^{-1} [31]), bulk/ionic nitrates at 1417 cm^{-1}

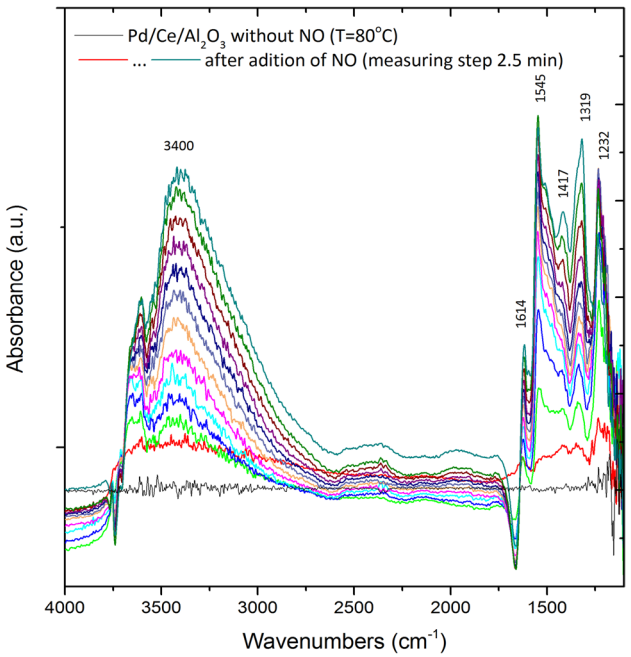

Fig. 6 DRIFTS spectra of Pd/Ce/Al_2O_3 recorded at 80 °C after exposure to NO with O_2 and H_2O in the gas mixture

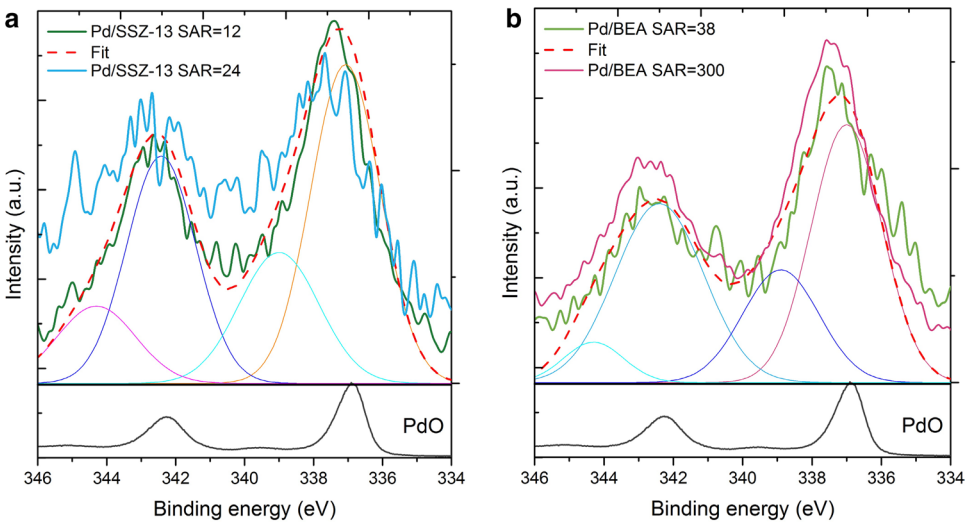

Fig. 5 Pd 3d XPS spectra of the fresh **a** Pd/SSZ-13 with SAR = 12 and SAR = 24, **b** Pd/BEA with SAR = 38 and SAR = 300

(1420 cm^{-1} [32]) and bridged nitrites at 1319 cm^{-1} (1320 cm^{-1} [30]). The identification of adsorption sites is problematic because Al_2O_3, Pd/Al_2O_3 and Pd/CeO_2 show bands in the same region [32–34]. The appearance of the broad band at higher frequencies, more specifically in the region of 2500–3800 cm^{-1} are associated various hydroxyl species [35]. Even though the catalyst was exposed for several hours to water and O_2, prior to adding NO, the hydroxyl groups continued to grow.

Figure 7 shows DRIFT spectra collected during NO adsorption on Pd/SSZ-13 with various SARs in the presence of O_2 and H_2O at 80 °C in the range of 1500–4000 cm^{-1}. The highest peaks are observed at 1818 and 1817 cm^{-1}, respectively (Fig. 7a, b). Moreover, a band with lower intensity is found at 1871–1872 cm^{-1}. According to Chakarova et al. [36], bands at 1881 and 1839 cm^{-1}, can be associated with nitrosyl complexes on palladium cations in Pd/ZSM-5, where 1881 cm^{-1} is assigned to Pd^{2+}–NO nitrosyls and 1839 cm^{-1} to $Pd^{2+}(H_2O)(NO)$. Based on these literature results, we assign our band at 1818 cm^{-1} to $Pd^{2+}(H_2O)(NO)$ nitrosyls and at 1871 cm^{-1} to Pd^{2+}–NO nitrosyls, respectively. These results are consistent with the work by Ryou et al. [22] that studied NO adsorption on Pd/SSZ-13 and found peaks at 1800 cm^{-1} with a shoulder at 1860 cm^{-1}, that they assigned to nitrosyl complexes on ionic Pd species. Moreover, according to Hess et al. [37], there are NO dimer species formed on Pd(111) giving a band at 1779 cm^{-1}. We observe bands in this region at 1724 and 1745 cm^{-1} for the two Pd/SSZ-13 samples and we suggest that these are originating from NO dimers on palladium. A possible reason for the differences observed between our study and the work by Hess et al. [37] is that large part of our palladium is in ion-exchanged positions and Pd particles while in the other work, Pd(111) surface was studied.

One broad area, with two overlapping broad bands were found in the region 2000–2400 cm^{-1}, for example for Pd/SSZ-13(SAR = 24) at 2112 and 2281 cm^{-1}. The band 2112 cm^{-1} is assigned to nitrosonium ions adsorbed onto different cationic positions in the zeolite framework [38–40]. Chen et al. [13] also observed a peak in this area for Pd/CHA in a similar region (2151 cm^{-1}) which they assign to NO^+ on Brønsted acid sites. However, this was in dry conditions, and when they added water this band disappeared, showing the instabilities of NO species associated directly with the zeolite structure. In our study the NO species associated with the zeolite structure grew also in the presence of water and the difference could be due to that we used lower water concentration and lower temperature compared to the study by Chen et al. [13]. Interestingly, we have an additional band at higher frequency, 2281 cm^{-1}, which is further shifted to 2433–2446 cm^{-1} for Pd/BEA (see Fig. 8). This band was not observed when exposing H/ZSM-5 to NO and O_2, only a band at 2128 cm^{-1} was found [41]. Thus, it is not likely that this band is associated with NO species on the zeolite. Moreover, this band was not available for $Pd/Ce/Al_2O_3$ (see Fig. 6), thus it is not related to Pd particles. A possible explanation for this band could be nitrosyl species that are interacting with the zeolite in close contact with the palladium ions. Moreover, the shift of this band to higher wave lengths for Pd/BEA is in accordance with the work by Chen et al. [13], where they found that some bands shifted upwards when increasing the pore-size of the zeolite.

During the first minutes of adsorption, the band associated with nitrosyls on ionic palladium (1817 and 1871 cm^{-1}) increased. Interestingly, after 9 min the peaks at ca 1872 and 1818 cm^{-1} start to reduce while the wide absorption bands in the region 2000–2500 cm^{-1} is becoming more visible, both for Pd/SSZ-13 and Pd/BEA. For example, in the case of Pd/SSZ-13 (SAR = 24) there is a distinctive increase in the two bands at 2281 and 2112 cm^{-1} with prolonged NO exposure. These results suggests that after building up Pd^{2+}–NO species there starts to become more interaction with NO in the interface between zeolite and palladium atoms.

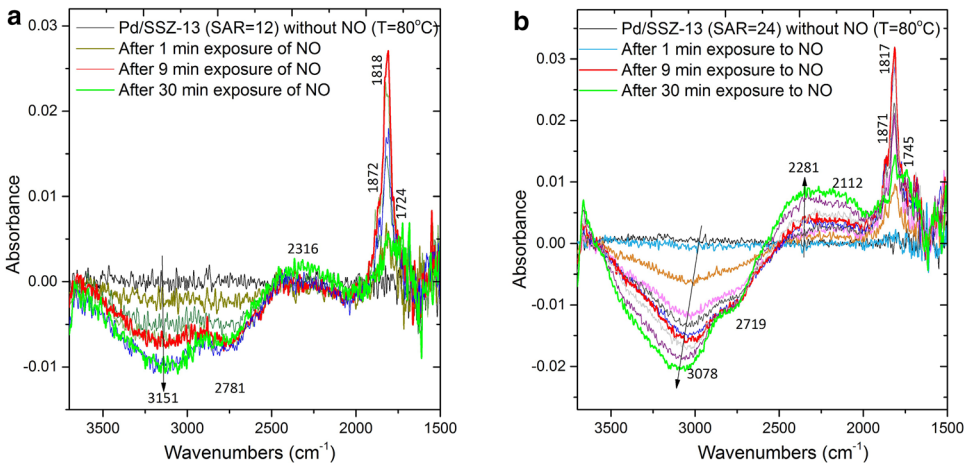

Fig. 7 DRIFTS spectra obtained during **a** Pd/SSZ-13 (SAR = 12) and **b** Pd/SSZ-13 (SAR = 24) exposure to NO under O_2 and H_2O at 80 °C

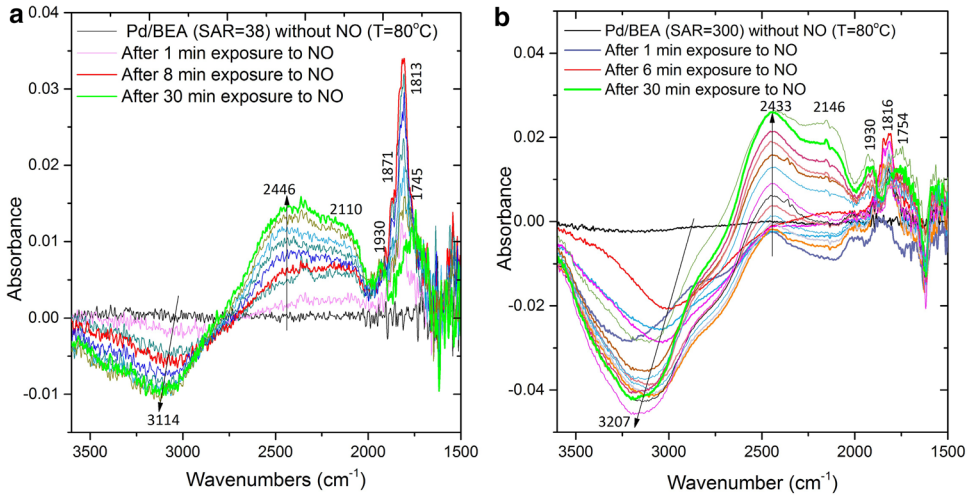

Fig. 8 NO DRIFTS spectra of **a** Pd/BEA (SAR = 38) and **b** Pd/BEA (SAR = 300)

Simultaneously as the NO was stored, the OH-groups (2500–3800 cm^{-1}) were removed. The build-up of hydroxyl groups and water adsorption on palladium is found in many studies and is a large problem for methane oxidation over Pd containing catalysts [42]. Fully hydrated a palladium ion can coordinate up to four water molecules [43]. It is well known that there are OH groups charge balancing the copper species ion-exchanged in Cu/SSZ-13, where $ZCu^{II}OH$ are formed (located in the 8MRs under non-reactive conditions [44]). In a similar way we propose that OH groups are also charge balancing the Pd species that are in ion-exchanged positions into the zeolite and there could also be water species adsorbed to the Pd sites. During NO adsorption some of these water species are pushed out, resulting in negative bands for the OH-groups. The XPS results (Fig. 4) showed large amount of Pd(II), which could originate from ion-exchanged palladium, which is in line with NO DRIFTS, where a clear band at 1818 cm^{-1} is observed due to nitrosyls on the Pd ions. This band in DRIFTS was not present for the $Pd/Ce/Al_2O_3$ showing that it is not occurring for NO adsorption on Pd particles.

There are quite large differences observed for NO adsorption on Pd/SSZ-13 with different SAR. For the Pd/SSZ-13 (SAR = 24) there is larger OH removal and in addition more NO species are associated with the zeolite structure and the interface between the structure and palladium. For the sample with low Si to Al ratio (SAR = 12, Fig. 7a) more Pd can bind to two Al, while for higher SAR there is less Al available and there will be a larger fraction of Pd binding to only one Al and charge balancing with OH groups. This results in that more OH-groups are removed for the sample with SAR = 24, which is clearly observed when comparing Fig. 7a, b.

The same experiment was conducted over Pd/BEA zeolites with SAR 38 and 300 and the results are shown in Fig. 8a, b, respectively. Pd/BEA (SAR = 38), exhibit many similarities with Pd/SSZ-13 samples, where the nitrosyls on Pd ions are growing, while the hydroxyl species are being removed. The peak at 2000–2200 cm^{-1} which is assigned to nitrosyls (NO^+) adsorbed on metal cations of the support [38–40] is growing more for Pd/BEA (SAR = 38) compared to Pd/SSZ-13 (SAR = 24) and finally Pd/SSZ-13 (SAR = 12) exhibit the smallest amount of this specie. Thus, it is clear that lowering the amount of Al in the sample increases this specie. In the same way as for Pd/SSZ-13, the peaks at ca 1813 and 1871 cm^{-1}, is first growing during first 6–8 min and thereafter decreasing, while the peaks at ca 2110 and 2446 cm^{-1} continues to grow. These results suggests that NO adsorbed on the ion-exchanged Pd sites, are transferred to also interact with the zeolite. When examining the results for Pd/BEA (SAR = 300), see Fig. 8b, there are quite large differences compared to Pd/BEA (SAR = 38) and the Pd/SSZ-13 samples. The main difference is that the peak at 1816 cm^{-1} is significantly smaller. This means that there is only a small amount of nitrosyl species on the ionic Pd, and this is reasonable since there are very few ionic exchange positions available for the palladium due to very small amount of Al.

3.3 NO TPD Experiments in Various Gas Mixtures

An important characteristic of PNA materials is that they should be able to adsorb and store large amount of NO_x at low temperature and release it preferably between 200–300 °C. This is investigated in this study by different TPD experiments by varying the feed composition. Figure 9 shows the results of the NO_x trapping at 80 °C followed by desorption phase with temperature ramp until 400 °C for $Pd/Ce/Al_2O_3$ catalyst. The NO concentration rapidly increases reaching the inlet NO concentration when H_2O is added to the ($NO + O_2$) feed mixture (Fig. 9b) compared to the ($NO + O_2$) TPD (Fig. 9a). Thus, it is clear that water inhibits the storage

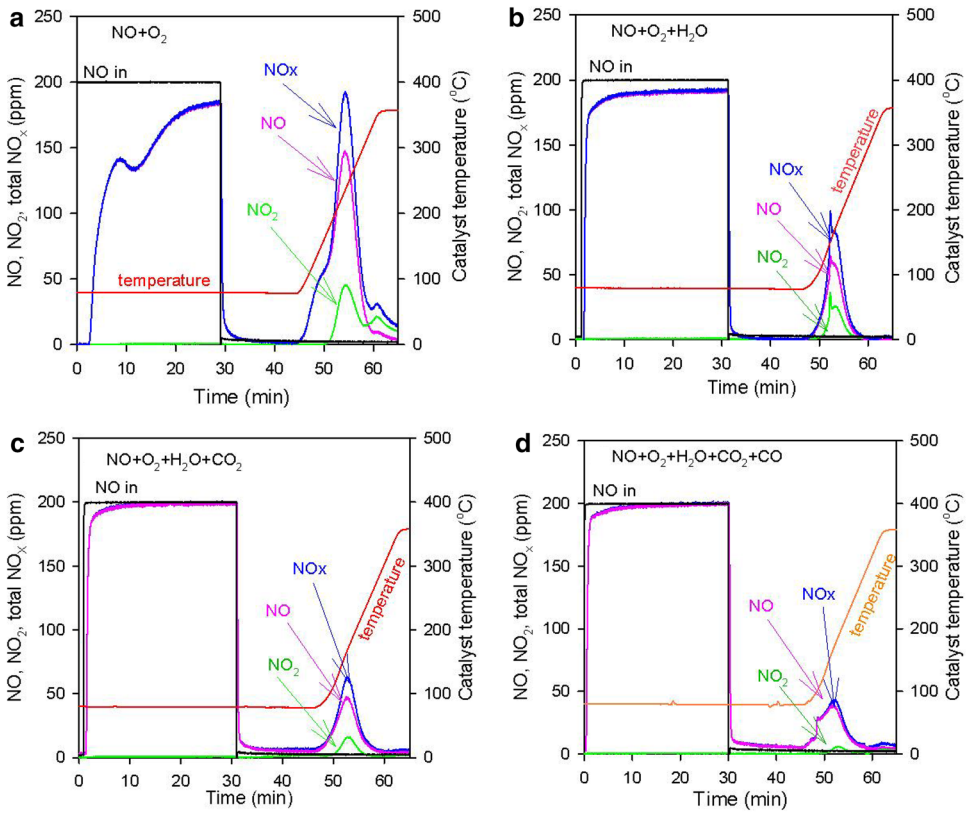

Fig. 9 TPD 1, 2, 3 and 4 (abbreviated in this study) over $Pd/Ce/Al_2O_3$ catalyst using **a** $NO+O_2$, **b** $NO+O_2+H_2O$, **c** $NO+O_2+H_2O+CO_2$ and **d** $NO+O_2+H_2O+CO_2+CO$. For experimental details see Table 2

and this negative water effect was also found by Zheng et al. [15] over Pd/zeolites. The addition of CO_2 also affects the storage negatively (see Fig. 9c). Moreover, there are some NO_2 detected in the reactor outlet during desorption. However, no NO_2 is visible during the adsorption phase. Thus we suggest that there are some nitrates formed that when decomposing forms NO_2. However, when CO was present during the storage, there was almost no NO_2 observed during the TPD (Fig. 9d), showing the inhibition effect of CO on the nitrate formation. Moreover, during desorption for the dry TPD experiment, three peaks are observed which is not the case for the $NO+O_2+H_2O+CO_2$ experiment. For example, the low temperature shoulder is not found in the presence of water and this could be that water disables the formation of loosely bound nitrates/nitrates. For the $NO+O_2+H_2O$ TPD there is one major peak, but with small sudden increase in the concentration, which likely originates from water fluctuation.

The NO_x storage profiles of Pd/SSZ-13 (SAR = 12) are presented in Fig. 10. Same adsorption–desorption event (see Fig. 9) was performed. The storage in dry conditions is significantly larger compared to in the presence of water also for this sample, in accordance with literature [15]. In addition, the CO addition increased the storage significantly (doubled the NO_x in the TPD), which is in line with the work by Vu et al. over Pd/BEA [17]. DRIFT studies indicate that CO addition lowers the oxidation state of the palladium, which results in that NO_x can bind more strongly due to π-back donation from Pd when the metal gets more electrons [17].

In order to easier facilitate comparison of the effect of different gases, the NO_x release profiles for $Pd/Ce/Al_2O_3$ and different Pd–zeolites are depicted in Fig. 11, after adsorption experiments at 80 °C in the presence of water. The addition of CO_2 has an important impact on Ce (Fig. 11a), where it decreases the storage and release. However, a similar trend was not found for BEA and SSZ-13-based materials (Fig. 11b, c), where the addition of CO_2 did not give any effect. The formation of cerium carbonates [45] in the presence of CO_2, could be the reason for the negative effect of CO_2 on $Pd/Ce/Al_2O_3$. As an example, the desorbed amount of NO_x for Pd/SSZ-13 (SAR = 12) was determined and we found 103 µmol of NO_x for the dry case, while for $NO+O_2+H_2O$ and $NO+O_2+H_2O+CO_2$, 6.8 and 7.0 µmol of NO_x were observed, which clearly shows the huge negative impact of water, while no effect of CO_2 addition.

Furthermore, the results presented in Fig. 11 show that the addition of CO influences the NO_x storage and desorption. CO is an important component since the PNA likely will be the first component in the aftertreatment system, and there will therefore be CO present during most conditions. CO has earlier found to be beneficial for NO trapping for Pd/BEA [17]. Interestingly, the addition of CO inhibits the NO_x storage over $Pd/Ce/Al_2O_3$ sample (Fig. 11a), whereas

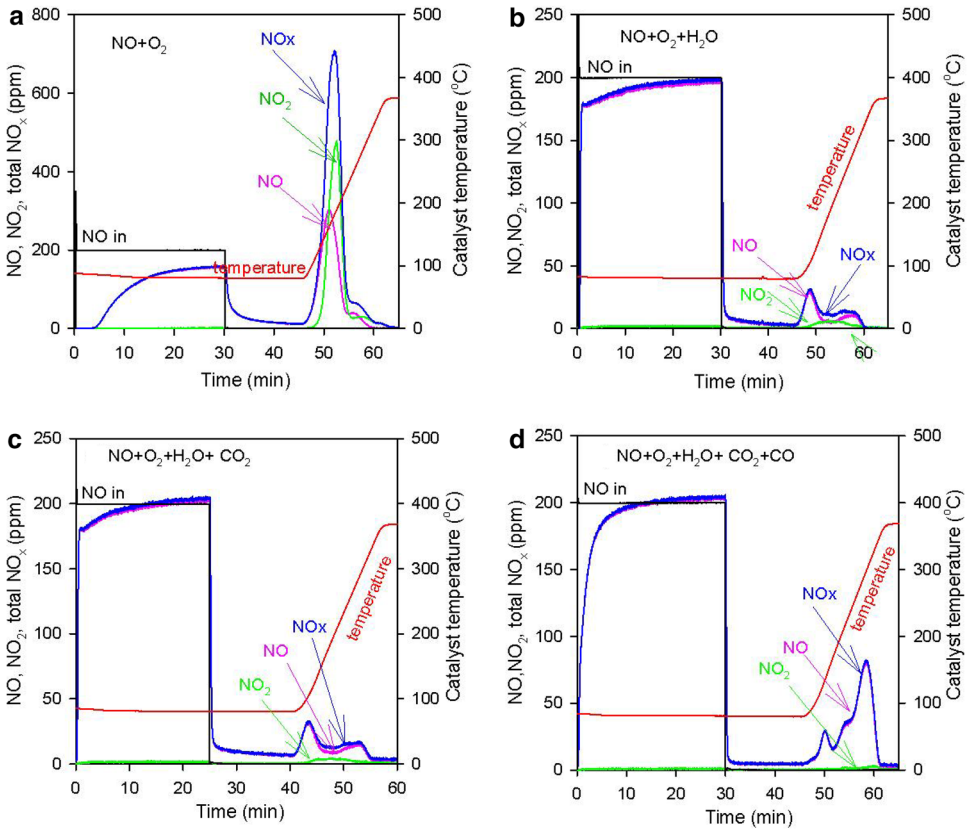

Fig. 10 TPD 1, 2, 3 and 4 over Pd/SSZ-13 (SAR = 12) using **a** $NO + O_2$, **b** $NO + O_2 + H_2O$, **c** $NO + O_2 + H_2O + CO_2$ and **d** $NO + O_2 + H_2O + CO_2 + CO$. For experimental details see Table 2

enhanced NO_x storage over the Pd–zeolites (Fig. 11b, c) were observed. For Pd/SSZ-13 (SAR = 12), the NO_x desorbed was 15.4 µmol, i.e. there is more than twice the amount of stored NO_x (if assuming all NO_x are released) in the presence of CO. This corresponds to 0.22 NO per palladium. Moreover, the storage was much more enhanced over the Pd/SSZ-13-catalyst than Pd/BEA. The presence of CO resulted in a shift in desorption temperature toward higher temperatures over the Pd/zeolites and now a large amount of NO_x is released in the optimum window (ca 200–300 °C). It should be noted that there are multiple desorption peaks for the Pd/zeolites (Fig. 11b–d), while only one for the Pd/Ce/Al_2O_3 sample. Multiple peaks were also found by Vu et al. [17], and using CO DRIFT experiments they concluded that there are both multiple Pd states, as well as multiple types of binding sites. This could explain that we observe multiple peaks for the Pd/zeolites.

Comparing similar Si to Al ratio (Fig. 11c, d), the effect of support (i.e. SSZ-13 and BEA) is clearly emphasized. There is large differences between the supports. For the experiments in the presence of $NO + O_2 + H_2O$ and $NO + O_2 + H_2O + CO_2$ there are two peaks at low and medium temperature and a high temperature shoulder for Pd/BEA (see Fig. 11b, d). However, for the Pd/SSZ-13 catalyst there is only two peaks present at low and high temperature. Interestingly, when adding CO during the storage especially the high temperature peak is enhanced, and for Pd/BEA the shoulder at high temperature is now the dominating peak. Interestingly, the CO has significantly larger effect on the Pd/SSZ-13 (SAR = 24) compared to Pd/BEA (SAR = 25), where the NO_x desorbed is a factor of 3.6 larger for Pd/SSZ-13.

The effect of Si to Al ratio for Pd/BEA in the absence/presence of CO in ($NO + O_2 + H_2O + CO_2$) mixture is studied and the results are presented in Fig. 12. Without the presence of CO, the Pd/BEA (see Fig. 12a) releases the NO_x in two desorption peaks around 100 and 180 °C, and an additional shoulder around 275 °C for the Pd/BEA (SAR = 25). Moreover, the low temperature peak is dominating for the Pd/BEA (SAR = 38), but the Pd/BEA (SAR = 300) stores less and have the main desorption peak at ca 180 °C. A possible reason for the poor PNA capacity of Pd/BEA (SAR = 300) is the lack of ion-exchanged Pd sites.

The addition of CO results in a high temperature desorption peak for Pd/BEA (SAR = 25 and SAR = 38), see Fig. 12b, as previously observed in literature for Pd/BEA [17]. This is due to that CO reduces the palladium and forms metallic Pd, "naked" Pd^{2+}, and Pd^{+} sites [15], where NO adsorption with higher binding energies occurs. Interestingly, there is no high temperature desorption peak found for Pd/BEA (SAR = 300), when the adsorption was conducted in the presence of CO (see Fig. 12b). The reason for this is also, as discussed in previous paragraph, that there is very

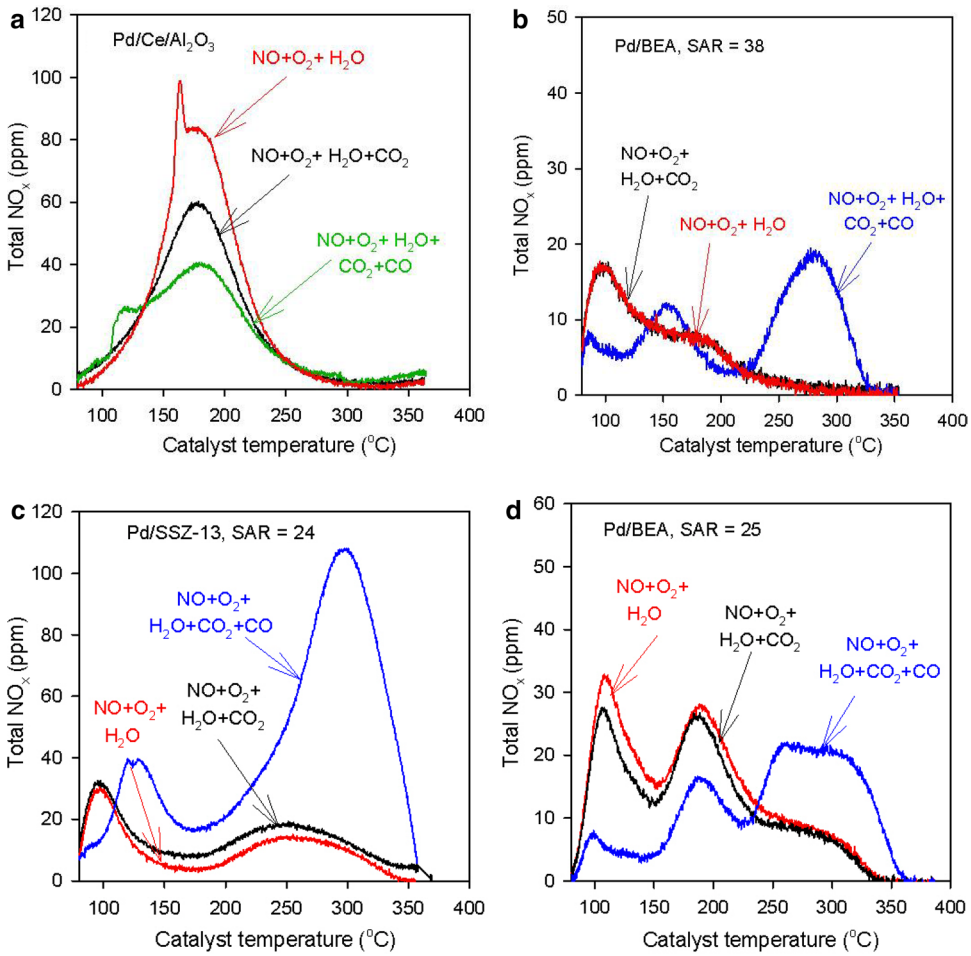

Fig. 11 NO_x desorption curves for ($NO+O_2+H_2O$) TPD, denoted TPD2, ($NO+O_2+H_2O+CO_2$) TPD as TPD3 and ($NO+O_2+H_2O+CO_2+CO$) TPD as TPD4 over **a** Pd/Ce/Al_2O_3, **b** Pd/BEA (SAR = 38), **c** Pd/SSZ-13 (SAR = 24) and **d** Pd/BEA (SAR = 25). For experimental details see Table 2

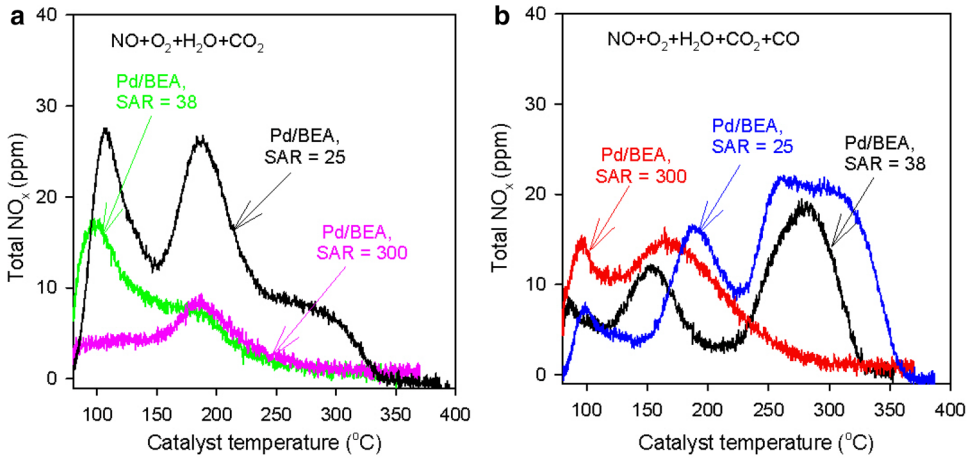

Fig. 12 NO_x desorption profiles of Pd/BEA (SAR = 25), Pd/BEA (SAR = 38) and Pd/BEA (SAR = 300), during **a** $NO+O_2+H_2O+CO_2$ TPD and **b** $NO+O_2+H_2O+CO_2+CO$ TPD experiments. For experimental details see Table 2

little ion-exchanged Pd available in this sample, as evident from the NO DRIFTS data (see Fig. 8b) and Pd mostly is in the form of Pd particles. For Pd/Ce/Al_2O_3, surprisingly, the CO addition was even negative (see Fig. 11a). To conclude, CO addition is beneficial when there is Pd available in ion-exchanged positions, which is the case for Pd/zeolites with low and medium SAR, and this result in Pd reduction and more stable NO_x species. However, for Pd/BEA with high SAR or Pd/Ce/Al_2O_3, the CO addition is not favorable.

The corresponding comparison for the NO_x desorption curves using Pd/SSZ-13 with different SAR are shown in Fig. 13. The results for Pd/SSZ-13(SAR = 12) and Pd/

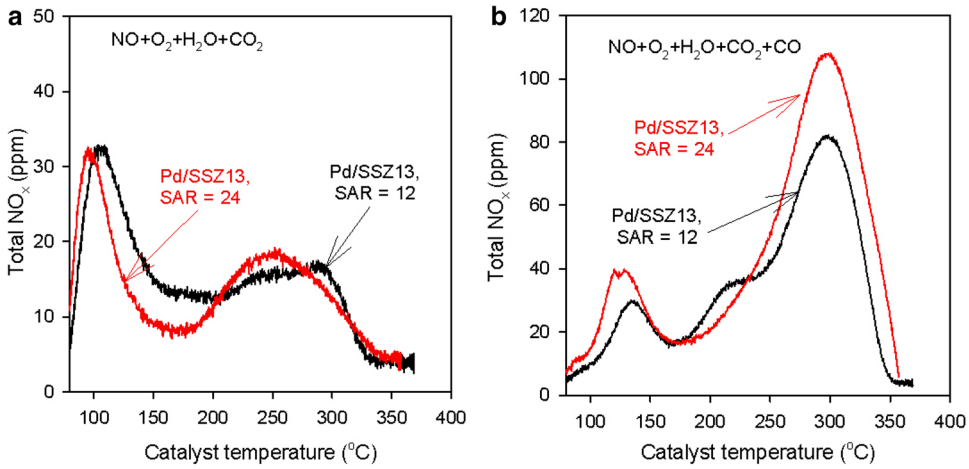

Fig. 13 NO_x desorption curves of Pd/SSZ-13 (SAR = 12) and Pd/SSZ-13 (SAR = 24) during **a** $NO + O_2 + H_2O + CO_2$ TPD and **b** $NO + O_2 + H_2O + CO_2 + CO$ TPD experiments. For experimental details see Table 2

SSZ-13(SAR = 24) is quite similar and this shows that there needs to be larger variations in the SAR ratio in order to see larger effects.

4 Conclusions

Pd/BEA and Pd/SSZ-13 with different SARs and Pd/Ce/Al_2O_3 as a base catalyst were synthesized and investigated for potential PNA use. The catalysts were characterized by BET, XRD, XPS, TPO, STEM and ICP-SFMS. The adsorbed NO species were examined using in-situ DRIFT spectroscopy and the adsorption/desorption characteristics were investigated using NO TPD experiments in various gas mixtures.

The TPO results showed that it required higher temperature to oxidize the Pd/zeolites than Pd/Ce/Al_2O_3. Moreover, the STEM showed that the Pd particles for Pd/BEA (SAR = 300) was significantly larger compared to the other zeolites with lower SAR for freshly calcined powder. However, after using the monoliths the Pd particles in Pd/BEA (SAR = 300) were reduced in size. The XPS data showed that in general for the Pd/zeolites there was large amount of Pd(II) and smaller amount of Pd(IV).

DRIFT spectroscopy revealed that on Pd/Ce/Al_2O_3 the NO was mainly stored as nitrates and nitrites in the region of 1600–1200 cm^{-1}. However, for the Pd/zeolites two peaks around 1800 cm^{-1} was found that relates to nitrosyl complexes on ionic Pd species. Moreover, a broad band in the region 2000–2500 cm^{-1} was observed, being more pronounced with increase in SARs. We assign these to nitrosyl species that interacts with zeolite structure, possibly in close connection with the Pd. In addition, hydroxyl species were found in the region 2500–3800 cm^{-1}. The catalyst had been pre-treated in H_2O and O_2 for several hours, both at high temperature and at the adsorption temperature (80 °C). However, when starting to introduce the NO, the OH-bands continued to grow on the Pd/Ce/Al_2O_3 sample, while they clearly decreased for the Pd/zeolites. We suggest that the reason for this is that for the Pd/zeolites there are palladium in ion-exchanged positions in the zeolite which is charge balanced with OH groups and also that there are water species adsorbed on these Pd species. This explains why there is such a negative impact during NO TPD experiments when adding water, since water blocks the Pd sites. In order to adsorb NO, NO must push out water species and this is the reason for that the OH-bands clearly decrease during NO adsorption over the Pd/zeolites.

Various NO TPD experiments were conducted and it was found that water significantly reduced the NO storage ability for all samples. Moreover, the addition of CO_2 to the $NO + O_2 + H_2O$ gas mixture decreased the storage on Pd/Ce/Al_2O_3 likely due to cerium carbonate formation, while it did not affect the Pd/zeolites. The addition of CO to $NO + O_2 + H_2O + CO_2$ resulted in interesting effects, where the effect differed if the palladium was in the form of Pd particles or in ion-exchanged positions and therefore also varied with Si/Al ratio.

The effect of SARs of the zeolites samples on the NO adsorption/desorption ability was studied. In $NO + O_2 + H_2O + CO_2$ TPD, the Pd/BEA samples released the NO_x at around 100 and 180 °C, for Pd/BEA (SAR = 38 and 300). However, for the Pd/BEA (SAR = 38) the low temperature peak is dominating, while this peak is very small for Pd/BEA (SAR = 300) and this sample also stores very little. Both these desorption peaks occur at too low temperature, since the optimum release temperature is between 200 and 300 °C. In addition, for Pd/BEA (SAR = 25) an extra shoulder was observed at higher temperature. Interestingly, when adding CO during the adsorption phase, the stored NO_x species for Pd/BEA (SAR = 25 and 38) is much more stable and is released at about 280 °C, but this peak is not existing for Pd/BEA (SAR = 300). This peak does also not e xist either on the Pd/Ce/Al_2O_3 sample, where actually the NO storage

is decreasing in the presence of CO. These results show that if the Pd is mostly in the form of particles, like for Pd/BEA (SAR = 300) and Pd/Ce/Al_2O_3, the CO addition is not beneficial. But if Pd is in ion-exchanged positions in the zeolite, the CO addition is beneficial because it helps to reduce the Pd species, which facilitate NO storage with higher binding energy. For both Pd/SSZ-13 samples (SAR = 12 and SAR = 24) there was a clear benefit of adding CO to the storage mixture, because also for these materials it increased the binding strength. Interestingly, the CO addition significantly increased the NO adsorption amount for Pd/SSZ-13, much more compared to the Pd/BEA. When comparing Pd/BEA (SAR = 25) with Pd/SSZ-13 (SAR = 24) it is clear that the Pd/SSZ-13 forms more NO_x species with higher stability and this was especially the case in the presence of CO.

Acknowledgements The funding from the Swedish Research Council (642-2014-5733) is acknowledged. This work was carried out at the Competence Centre for Catalysis and Chemical Engineering, Chalmers University of Technology. We acknowledge the help from Stefan Gustafsson, Division of Applied Physics at the Chalmers University of Technology for STEM measurements.

References

1. Körfer T (2013) Potential of advanced, combined aftertreatment systems for light-duty diesel engines to meet upcoming EU and US emission regulation, SAE International
2. Roy S, Baiker A (2009) Chem Rev 109:4054–4091
3. Epling WS, Campbell LE, Yezerets A, Currier NW, Parks JE (2004) Catal Rev 46:163–245
4. Olsson L, Wijayanti K, Leistner K, Kumar A, Joshi SY, Kamasamudram K, Currier NW, Yezerets A (2016) Appl Catal B 183:394–406
5. Forzatti P, Nova I, Tronconi E (2010) Ind Eng Chem Res 49:10386–10391
6. Beale AM, Gao F, Lezcano-Gonzalez I, Peden CHF, Szanyi J (2015) ChemSocRev 44:7371–7405
7. Lundström A, Andersson B, Olsson L (2009) Chem Eng J 150:544–550
8. Jones S, Ji Y, Bueno-Lopez A, Song Y, Crocker M (2017) Emiss Control Sci Technol 3:59–72
9. Tamm S, Andonova S, Olsson L (2014) Catal Lett 144:674–684
10. Ji Y, Bai S, Crocker M (2015) Appl Catal B 170–171:283–292
11. Ren SX, Schmieg SJ, Koch CK, Qi GS, Li W (2015) Catal Today 258:378–385
12. Melville JE, B RJ, K O, P PR, Mountstevens EH (2012) Johnson Matthey Public Limited Company, Royston
13. Chen H-Y, Collier JE, Liu D, Mantarosie L, Durán-Martín D, Novák V, Rajaram RR, Thompsett D (2016) Catal Lett 146:1706–1711
14. Theis JR, Lambert CK (2015) Catal Today 258:367–377
15. Zheng Y, Kovarik L, Engelhard MH, Wang Y, Wang Y, Gao F, Szanyi J (2017) J Phys Chem C 121:15793–15803
16. Lee J, Ryou Y, Cho SJ, Lee H, Kim CH, Kim DH (2018) Appl Catal B 226:71–82
17. Vu A, Luo J, Li J, Epling WS (2017) Catal Lett 147:745–750
18. McEwen JS, Anggara T, Schneider WF, Kispersky VF, Miller JT, Delgass WN, Ribeiro FH (2012) Catal Today 184:129–144
19. Olsson L, Wijayanti K, Leistner K, Kumar A, Joshi SY, Kamasamudram K, Currier NW, Yezerets A (2015) Appl Catal B 174–175:212–224
20. Franchini CA, Cesar DV, Schmal M (2010) Catal Lett 137:45–54
21. Lim JB, Jo D, Hong SB (2017) Appl Catal B 219:155–162
22. Ryou Y, Lee J, Lee H, Kim CH, Kim DH (2017) Catal Today 297:53–59
23. Kamińska II, Lisovytskiy D, Casale S, Śrębowata A, Dzwigaj S (2017) Microporous Mesoporous Mater 237:65–73
24. Tidahy HL, Siffert S, Lamonier JF, Zhilinskaya EA, Aboukaïs A, Su BL, Canet X, Deweireld G, Frère M, Gireaudon JM, Leclercq G (2007) Characterisation of palladium supported on exchanged BEA and FAU zeolites for VOCs catalytic oxidation. In: Llewellyn PL, Rodriquez-Reinoso F, Rouqerol J, Seaton N (Eds.) Studies in surface science and catalysis. Elsevier, New York
25. Yamanaka N, Itakura M, Kiyozumi Y, Ide Y, Sadakane M, Sano T (2012) Microporous Mesoporous Mater 158:141–147
26. Wang Y, Chen J, Lei X, Ren Y, Wu J (2018) Adv Powder Technol 29:1112–1118
27. Higgins JB, LaPierre RB, Schlenker JL, Rohrman AC, Wood JD, Kerr GT, Rohrbaugh WJ (1988) Zeolites 8:446–452
28. Leistner K, Brüsewitz F, Wijayanti K, Kumar A, Kamasamudram K, Olsson L (2017) Energies 10:489
29. Sadokhina N, Smedler G, Nylén U, Olofsson M, Olsson L (2017) Appl Catal B 200:351–360
30. Westerberg B, Fridell E (2001) J Mol Catal 165:249–263
31. Theologides CP, Olympiou GG, Savva PG, Kapnisis K, Anayiotos A, Costa CN (2017) Appl Catal B 205:443–454
32. Nova I, Castoldi L, Lietti L, Tronconi E, Forzatti P, Prinetto F, Ghiotti G (2004) J Catal 222:377–388
33. Auvray X, Olsson L (2015) Appl Catal B 168:342
34. Ryou Y, Lee J, Lee H, Kim CH, Kim DH (2018) Catal Today 307:93–101
35. Ciuparu D, Perkins E, Pfefferle L (2004) Appl Catal A 263:145–153
36. Chakarova K, Ivanova E, Hadjiivanov K, Klissurski D, Knozinger H (2004) Phys Chem Chem Phys 006:3702–3709
37. Hess C, Ozensoy E, Yi CW, Goodman DW (2006) J Am Chem Soc 128:2988–2994
38. Hadjiivanov K, Saussey J, Freysz JL, Lavalley JC (1998) Catal Lett 52:103–108
39. Sedlmair C, Gil B, Seshan K, Jentys A, Lercher JA (2003) Phys Chem Chem Phys 5:1897–1905
40. Szanyi J, Hun Kwak J, Moline RA, Peden CHF (2003) Phys Chem Chem Phys 5:4045–4051
41. Lonyi F, Solt HE, Valyon J, Decolatti H, Gutierrez LB, Miro E (2010) Appl Catal B 100:133–142
42. Sadokhina N, Ghasempour F, Auvray X, Smedler G, Nylen U, Olofsson M, Olsson L (2017) Catal Lett 147:2360–2371
43. Akesson R, Pettersson LGM, Sandstrom M, Wahlgren U (1994) J Am Chem Soc 116:8691–8704
44. Paolucci C, Parekh AA, Khurana I, Di Iorio JR, Li H, Albarracin Caballero JD, Shih AJ, Anggara T, Delgass WN, Miller JT, Ribeiro FH, Gounder R, Schneider WF (2016) J Am Chem Soc 138:6028–6048
45. Chengwu Y, Fabian B, Jun C, Xiaojuan Y, Alexei N, Christof W (2017) ChemPhysChem 18:1874–1880